

Figure 2. Tensile elastic modulus of polymer as function of temperature

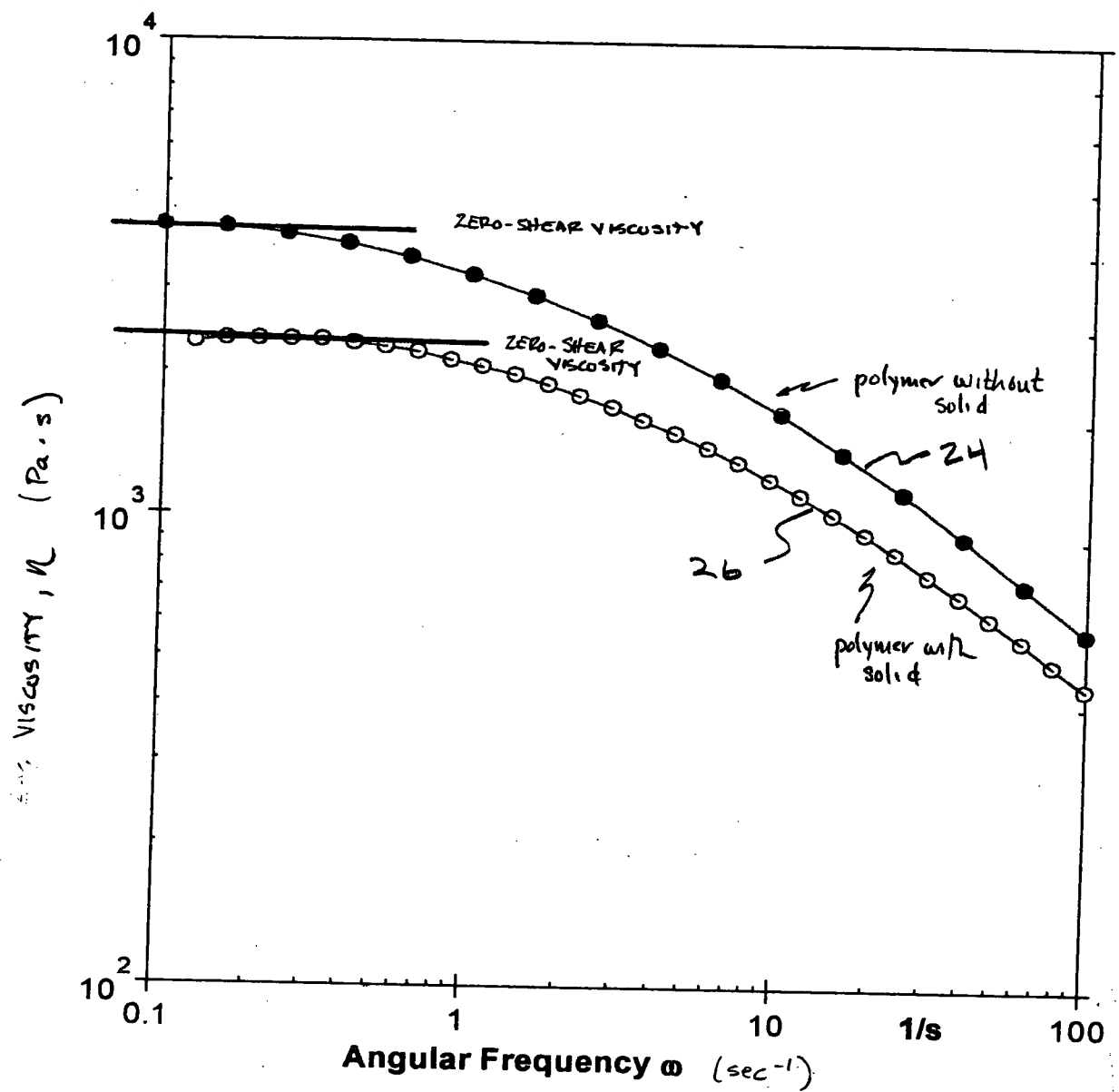


Figure 3. Determination of zero-shear viscosity from viscosity-frequency plot

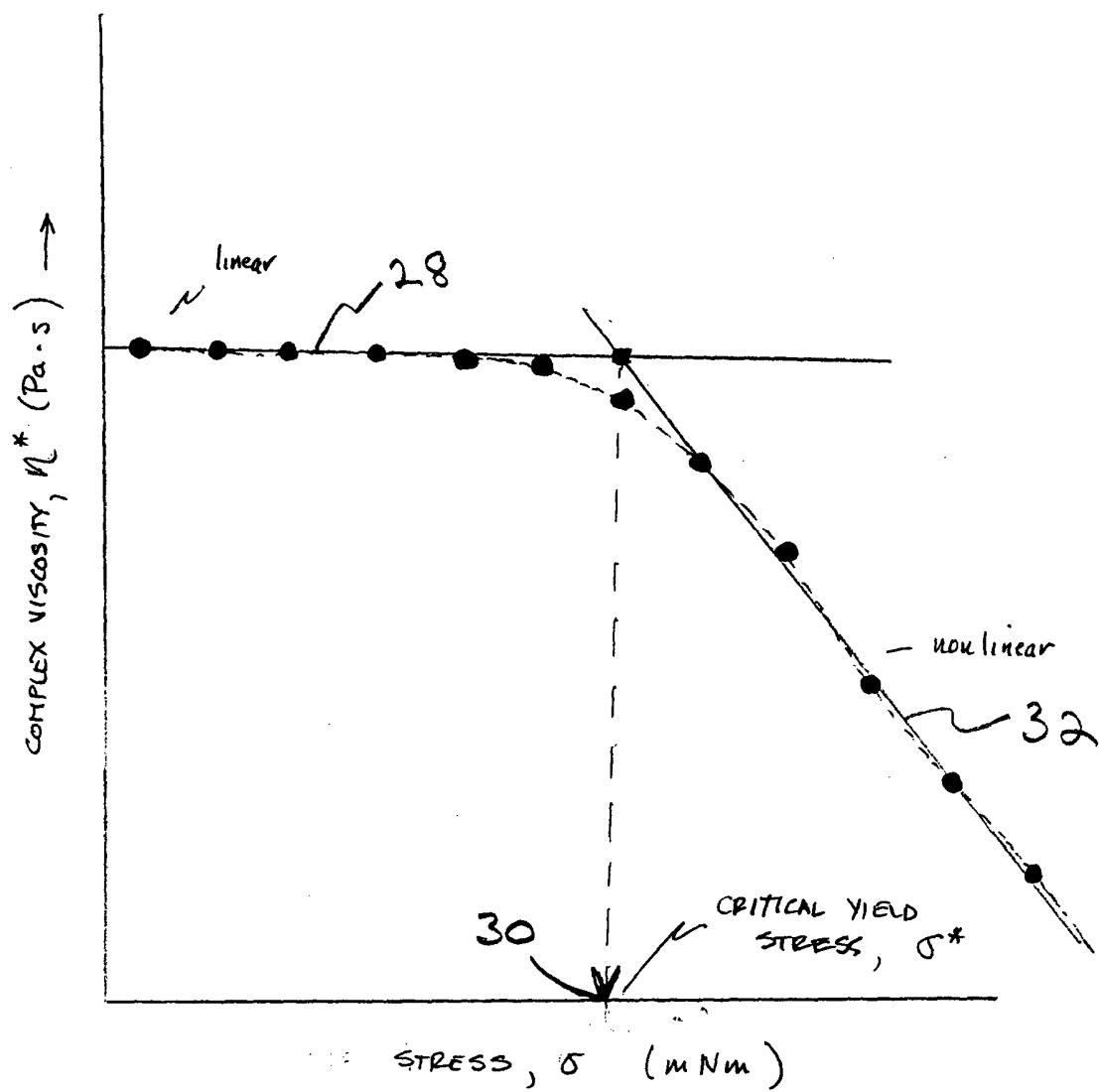


Figure 4. Determination of critical stress value from viscosity-stress curves.

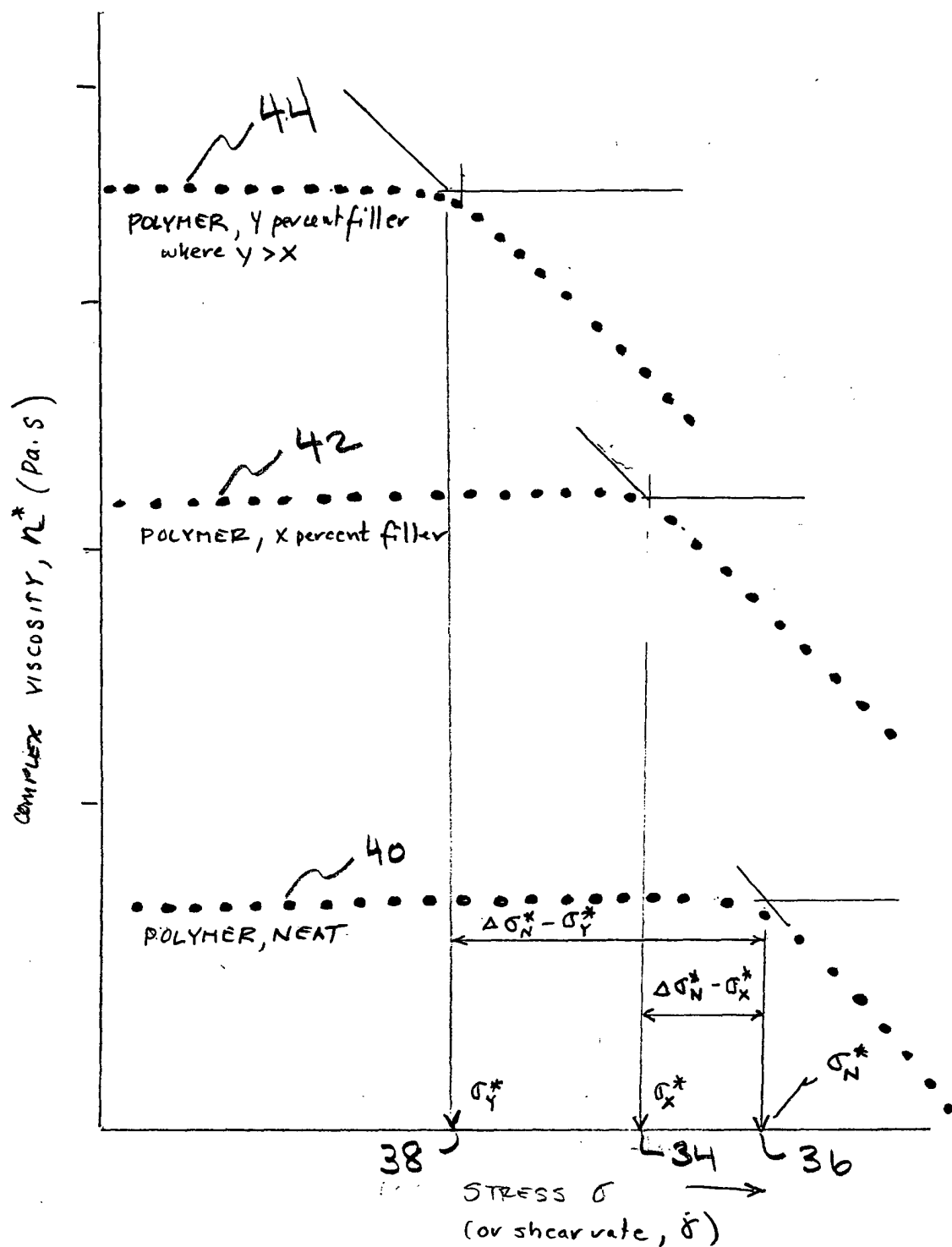
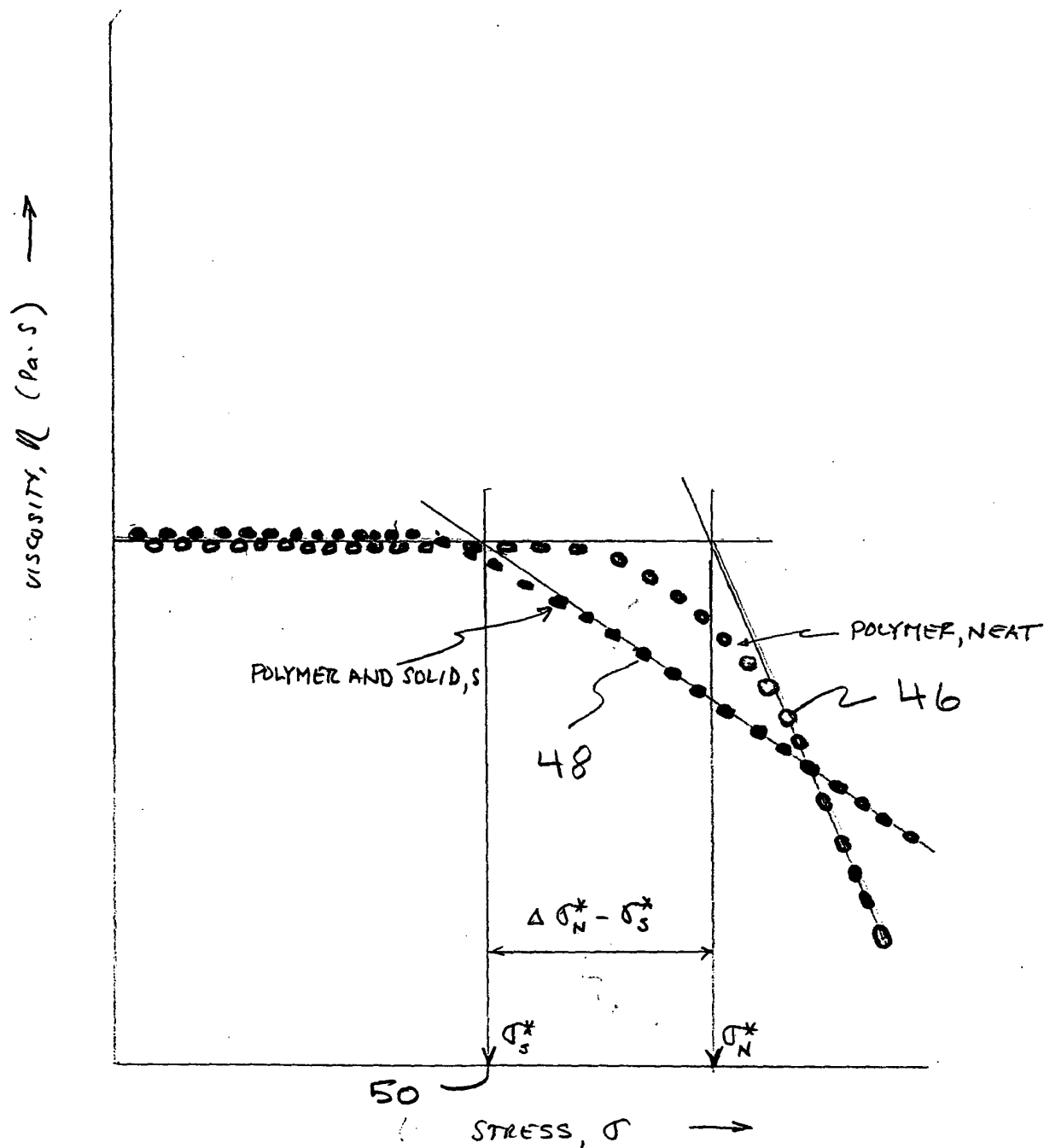


FIGURE 5. Effect of filler concentration on viscosity and critical stress value



on critical stress value by
 FIGURE 6. Effect of adding solid with preferred
 size range and concentration to NEAT polymer

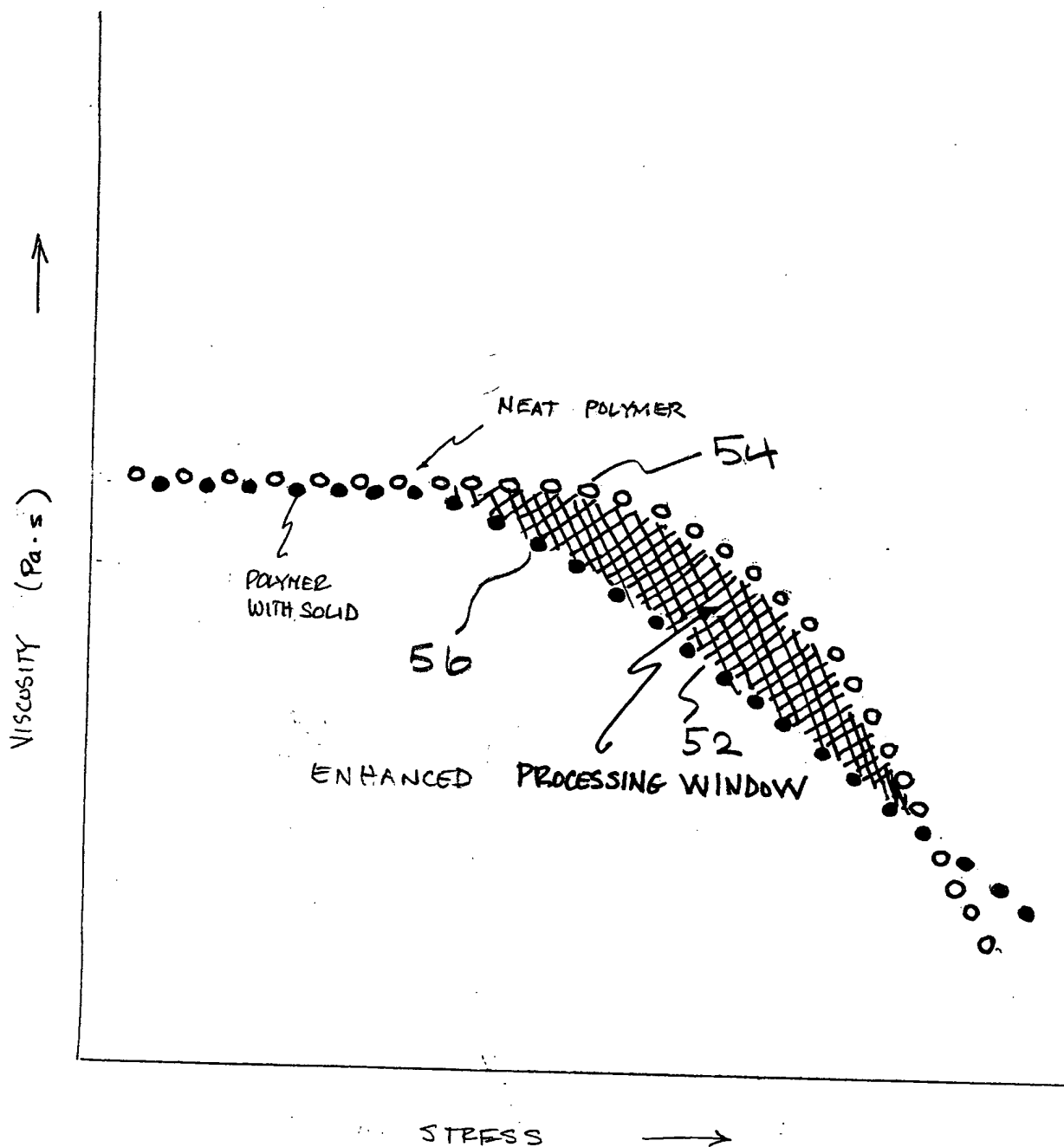


Figure 7. Processing window for unfilled polymers

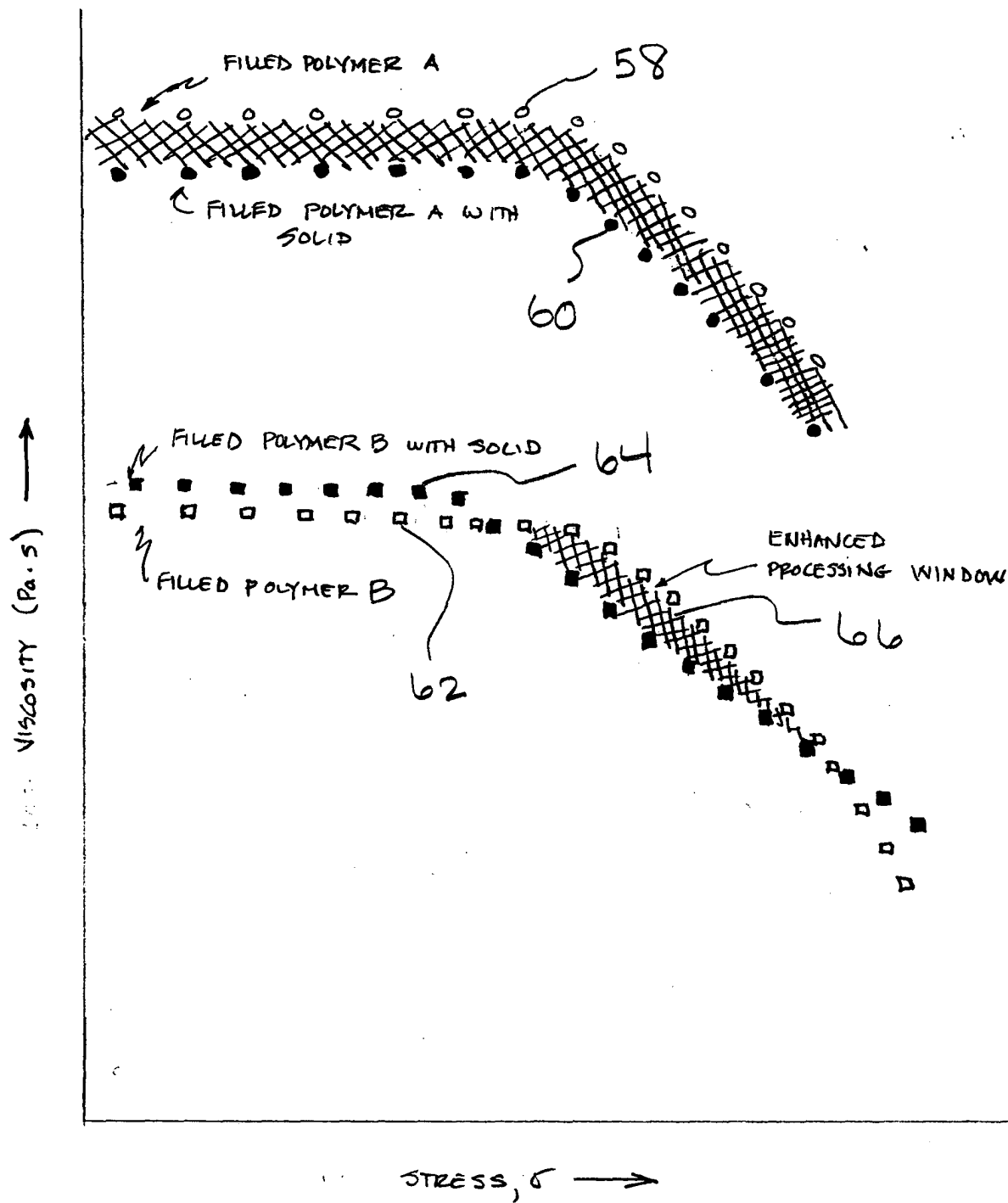


Figure 8. Processing window of filled polymers

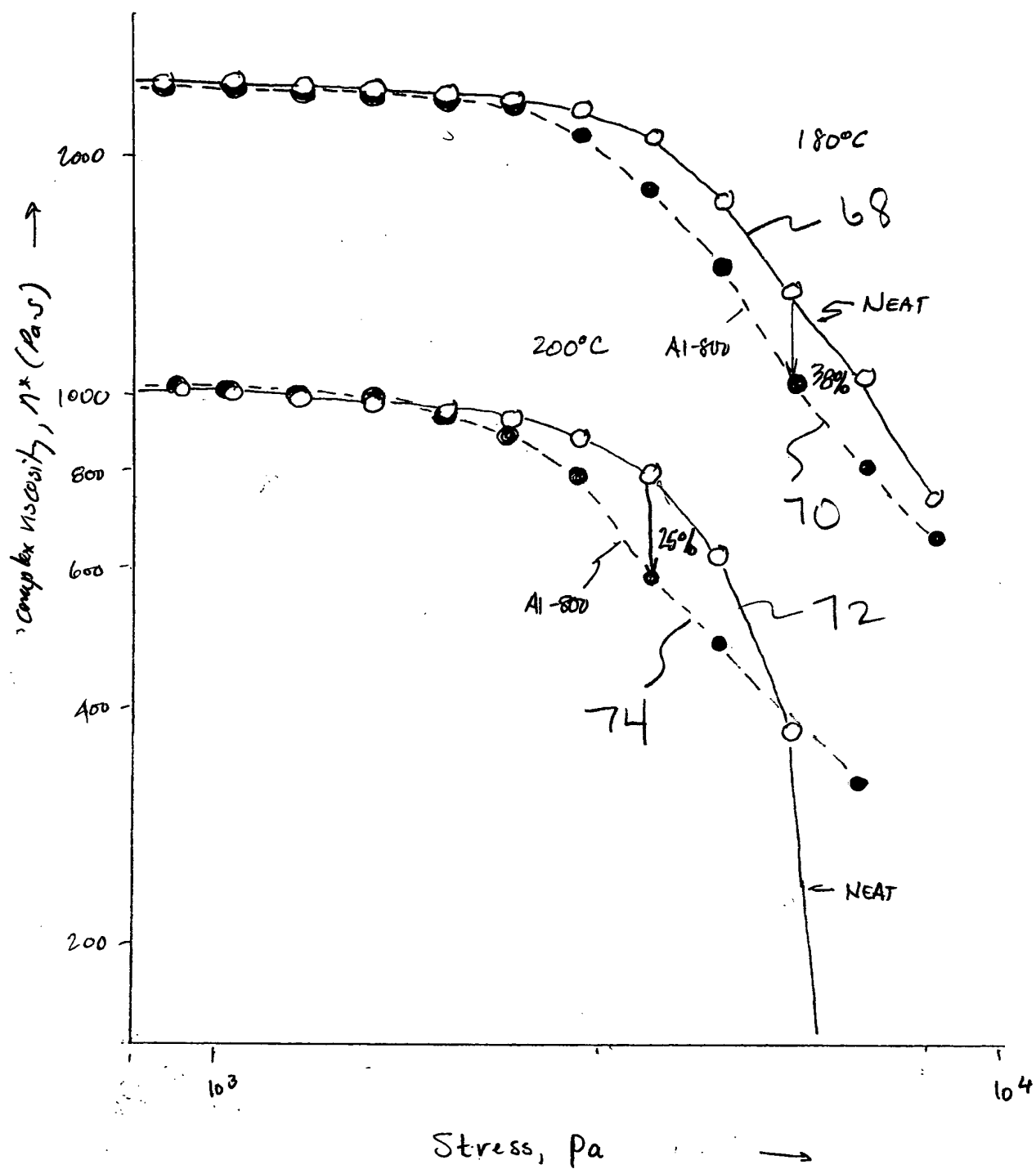


Figure 9. Complex viscosity of amorphous solid
Al-800 and NEAT PP

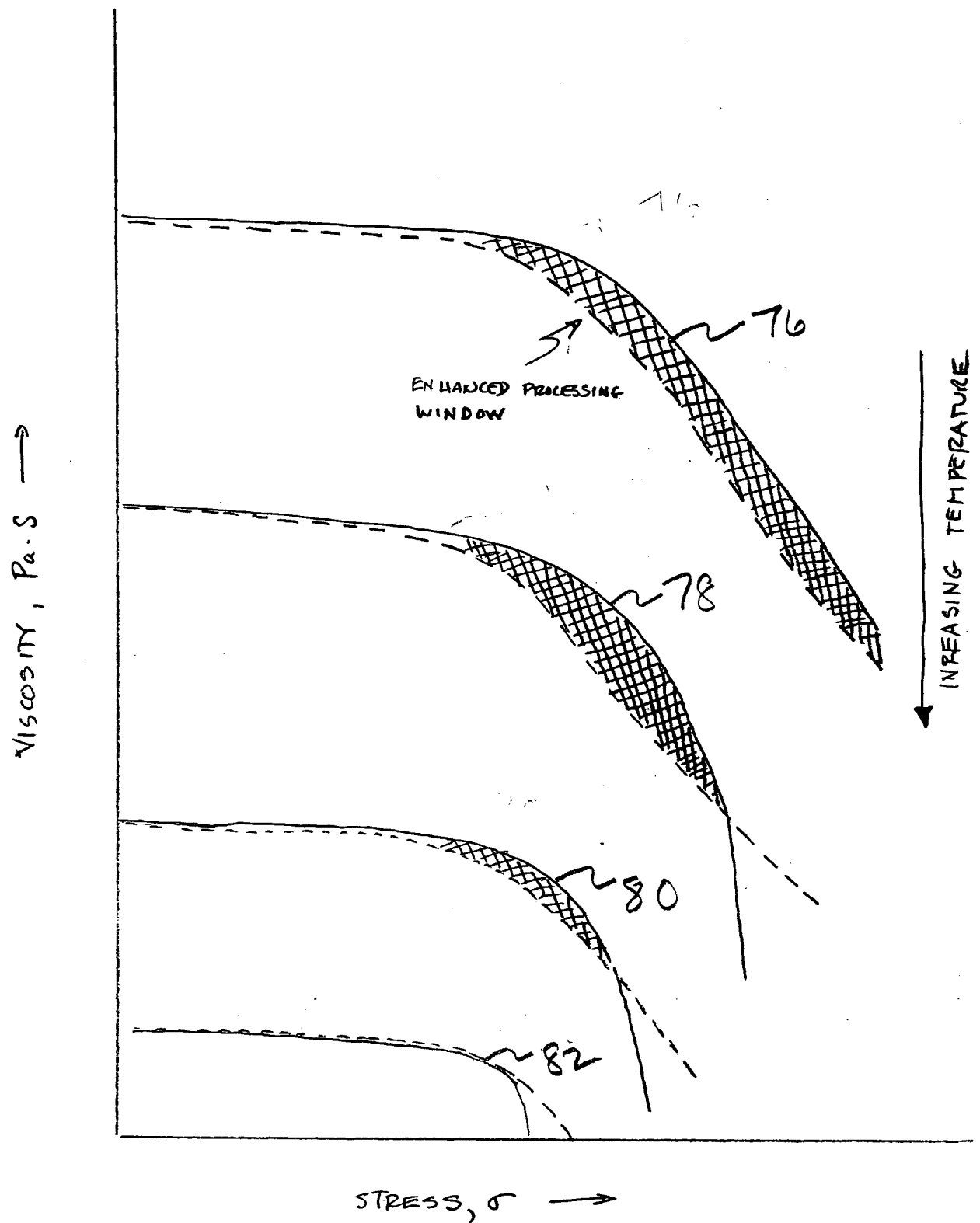


Figure 10. Effect of increasing temperature on enhanced processing window

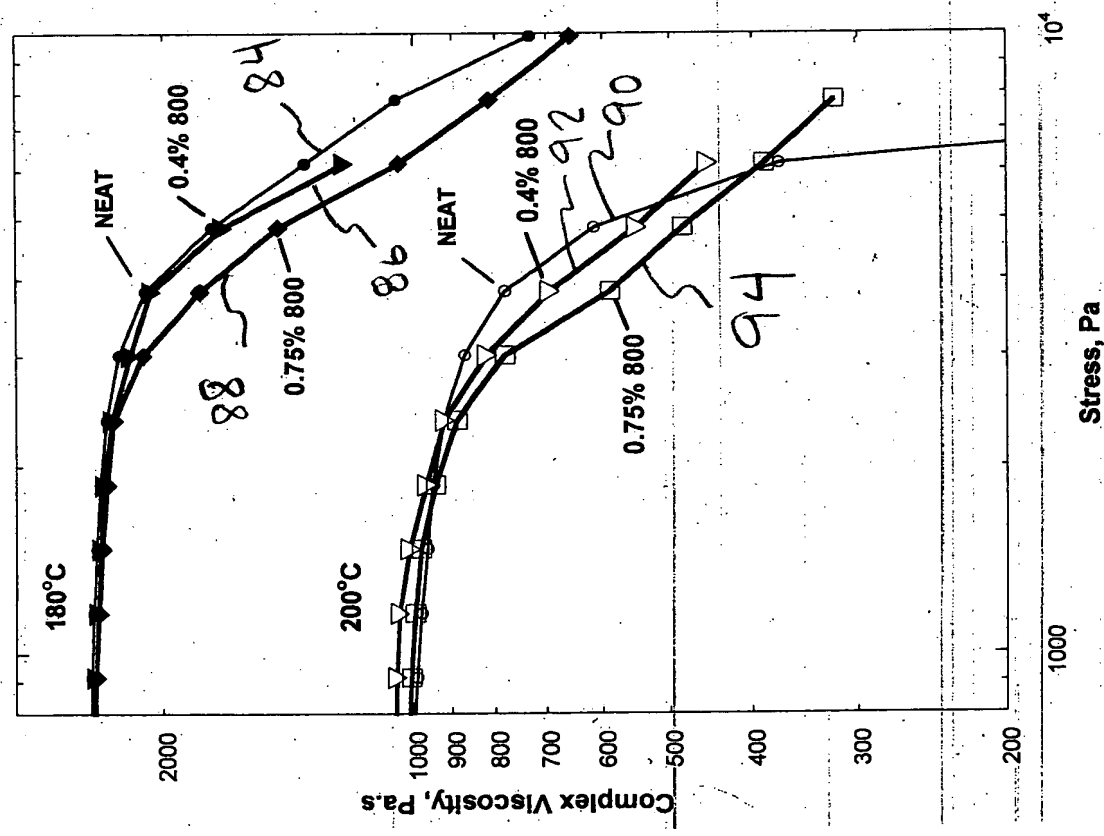
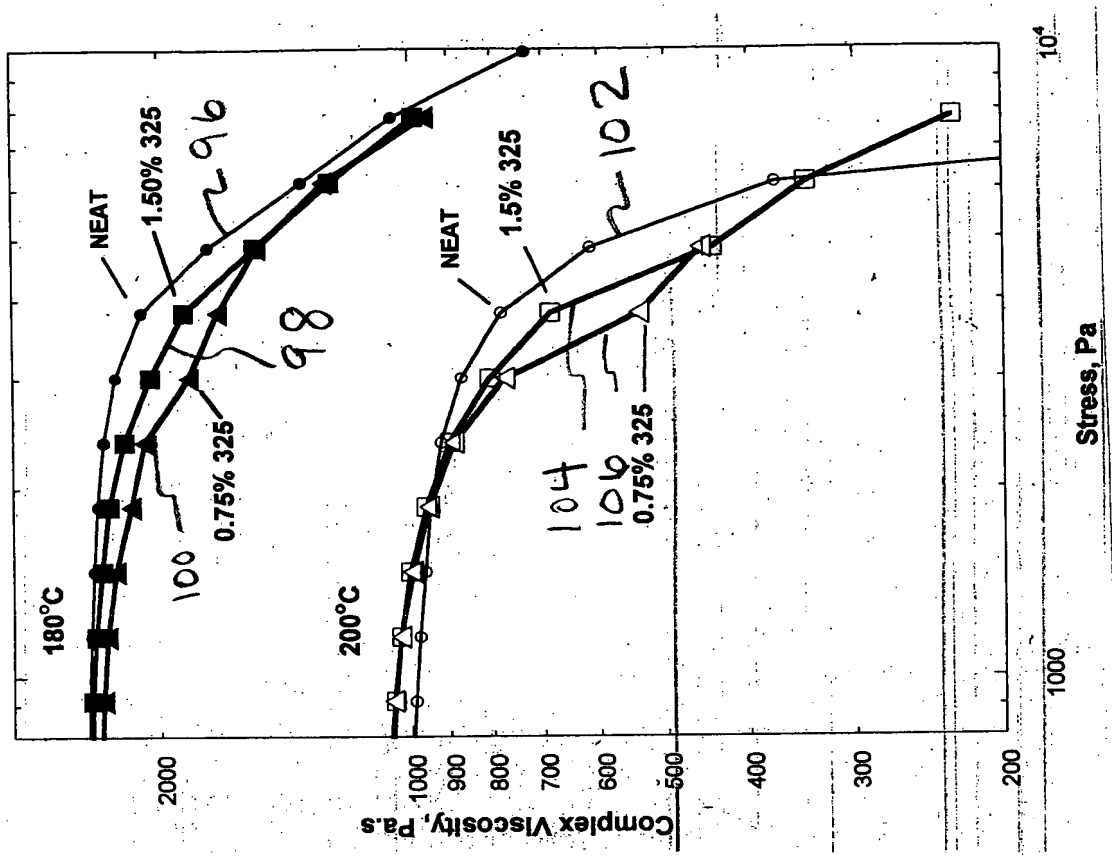


Figure 11. Effect of solid concentration on complex viscosity

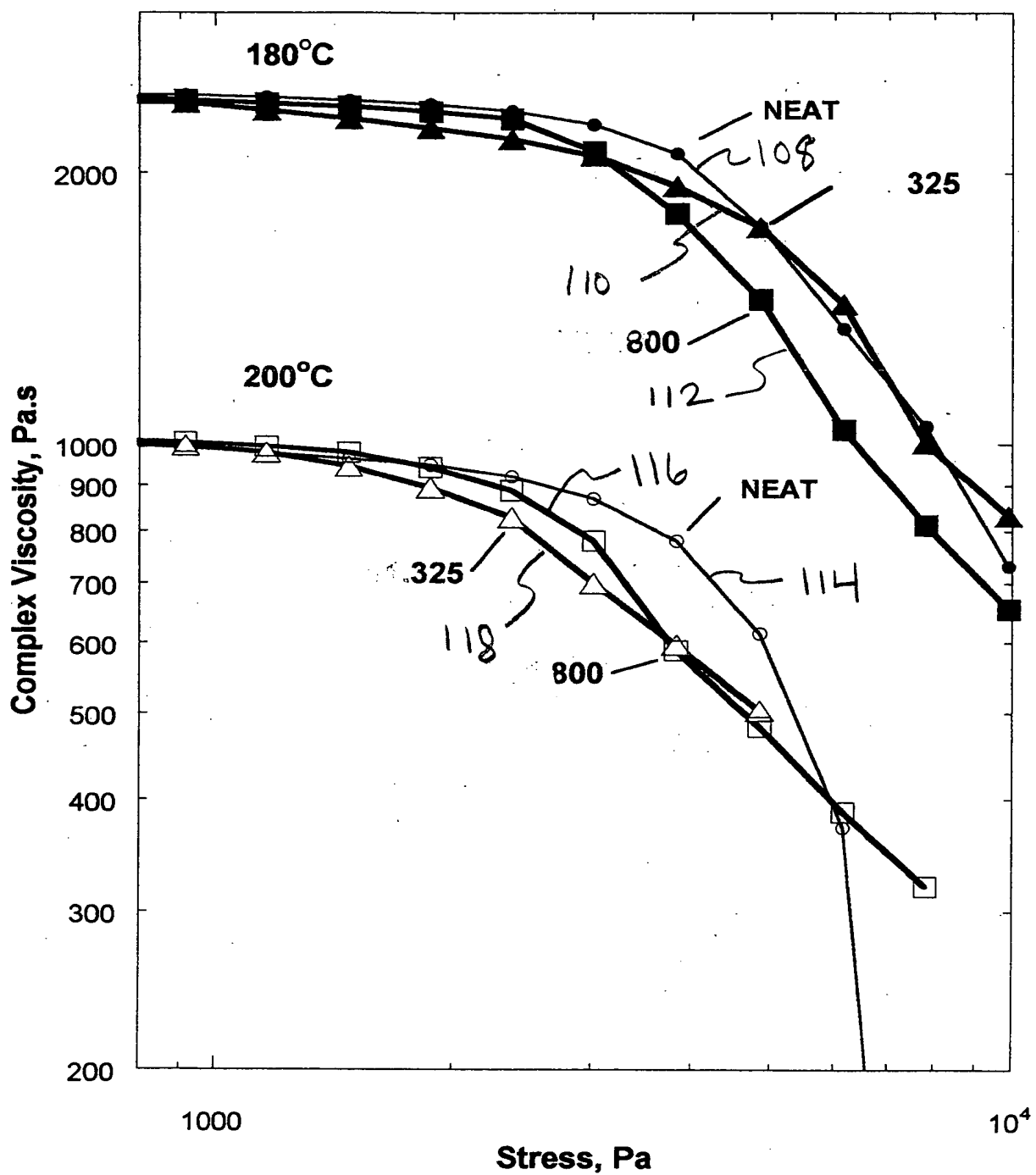


Figure 12. Effect of particle mesh size on complex viscosity

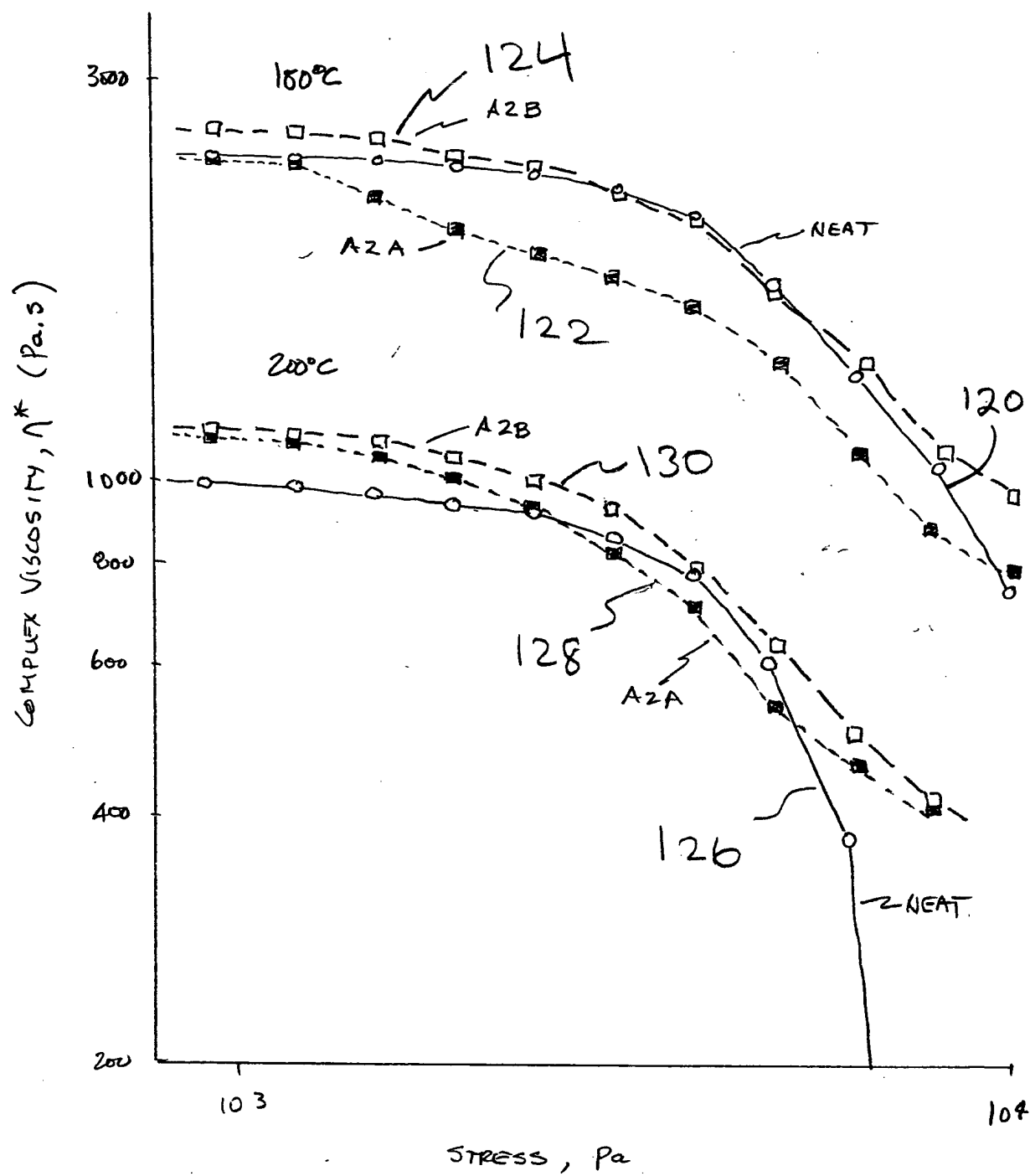


Figure 13. Complex viscosity of Eco-mesh amorphous solid A2 with different particle shapes

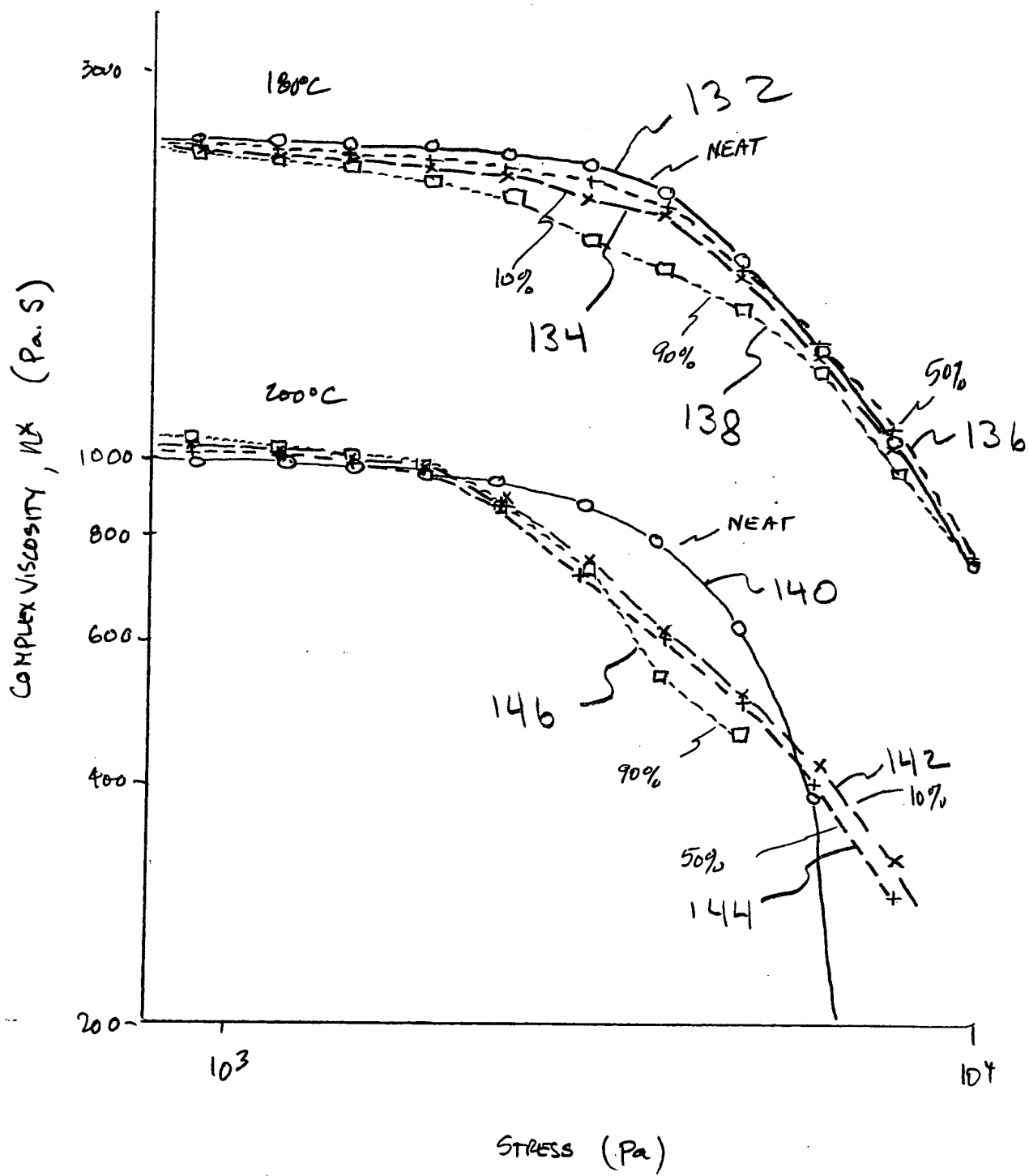


Figure 14. Effect of glass content on complex viscosity.

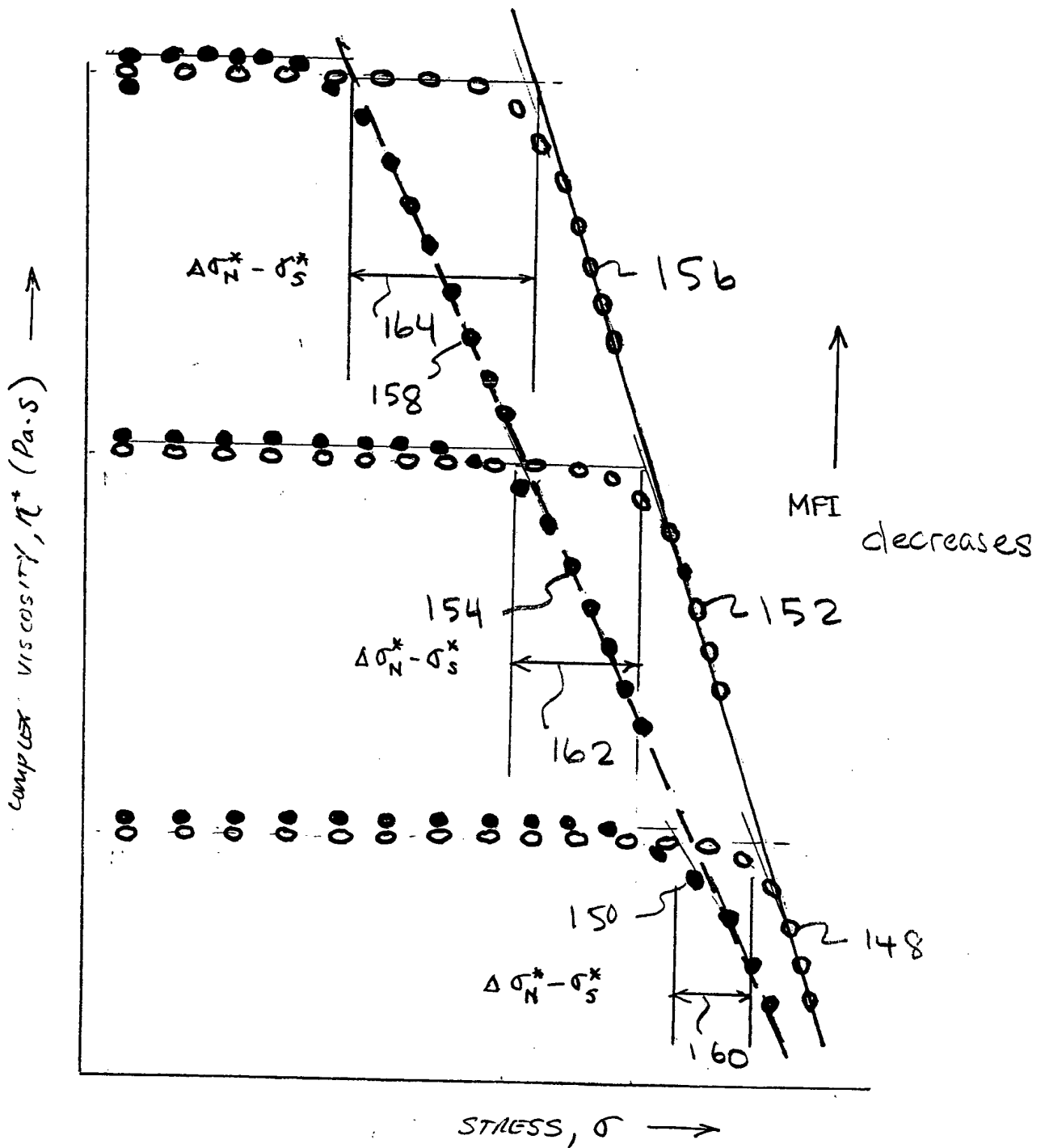


FIGURE 15. Variation in $\Delta\sigma_N^* - \sigma_S^*$ as a function of increasing MFI for a given polymer type.

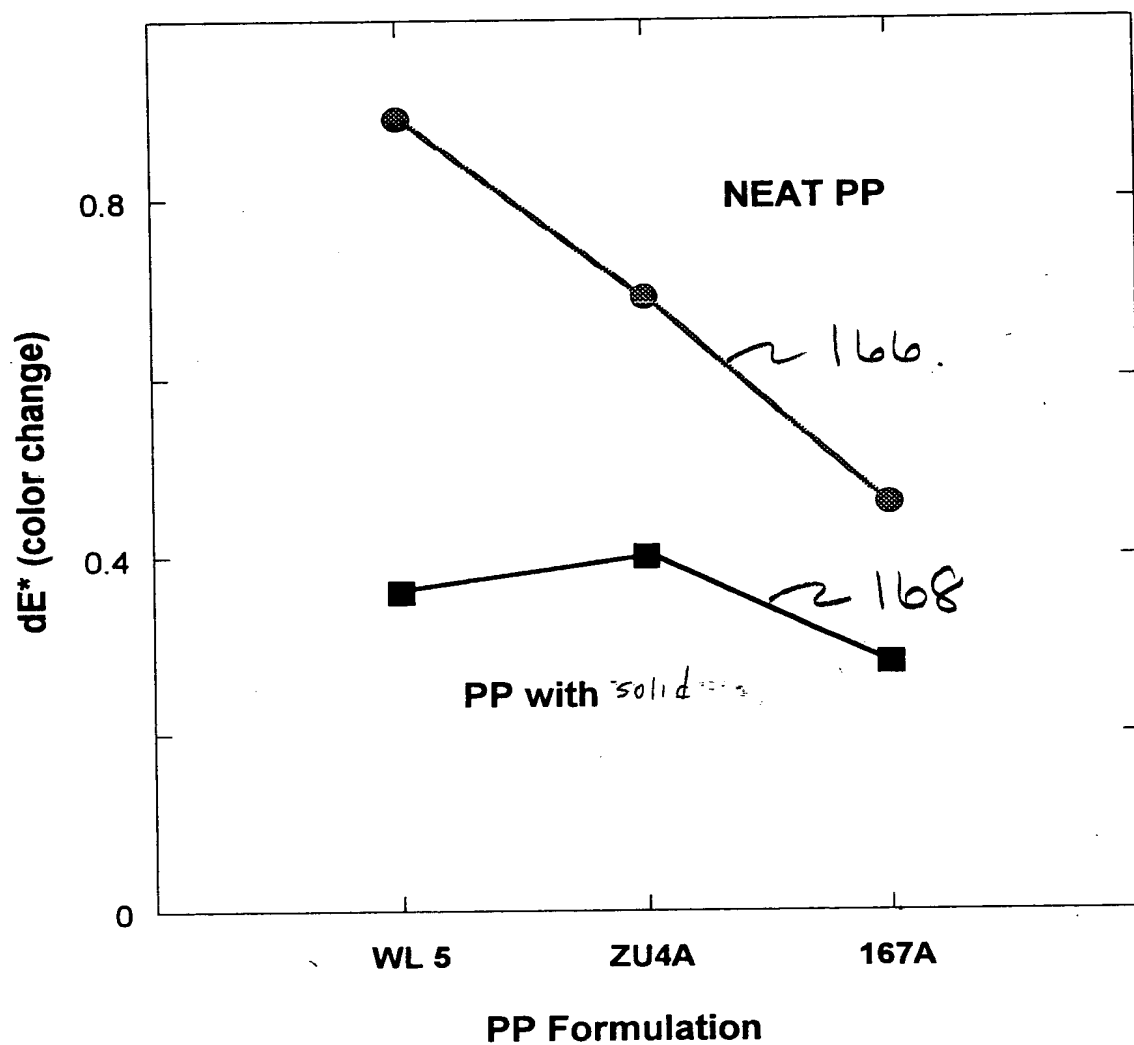


Figure 16. Color change (dE^*) in polypropylene after UV light exposure.

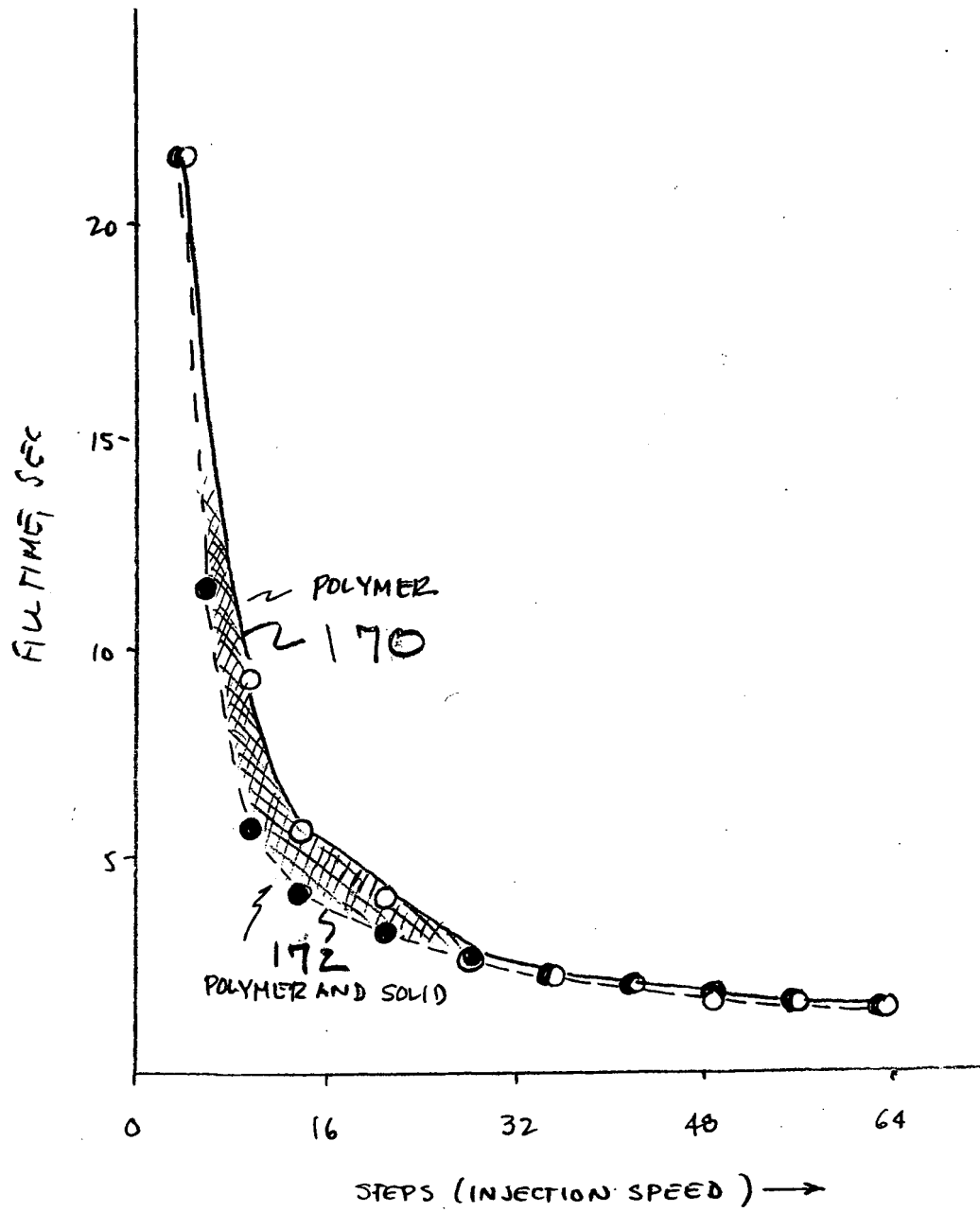


Figure 17. Effect of injection speed on mold fill time.

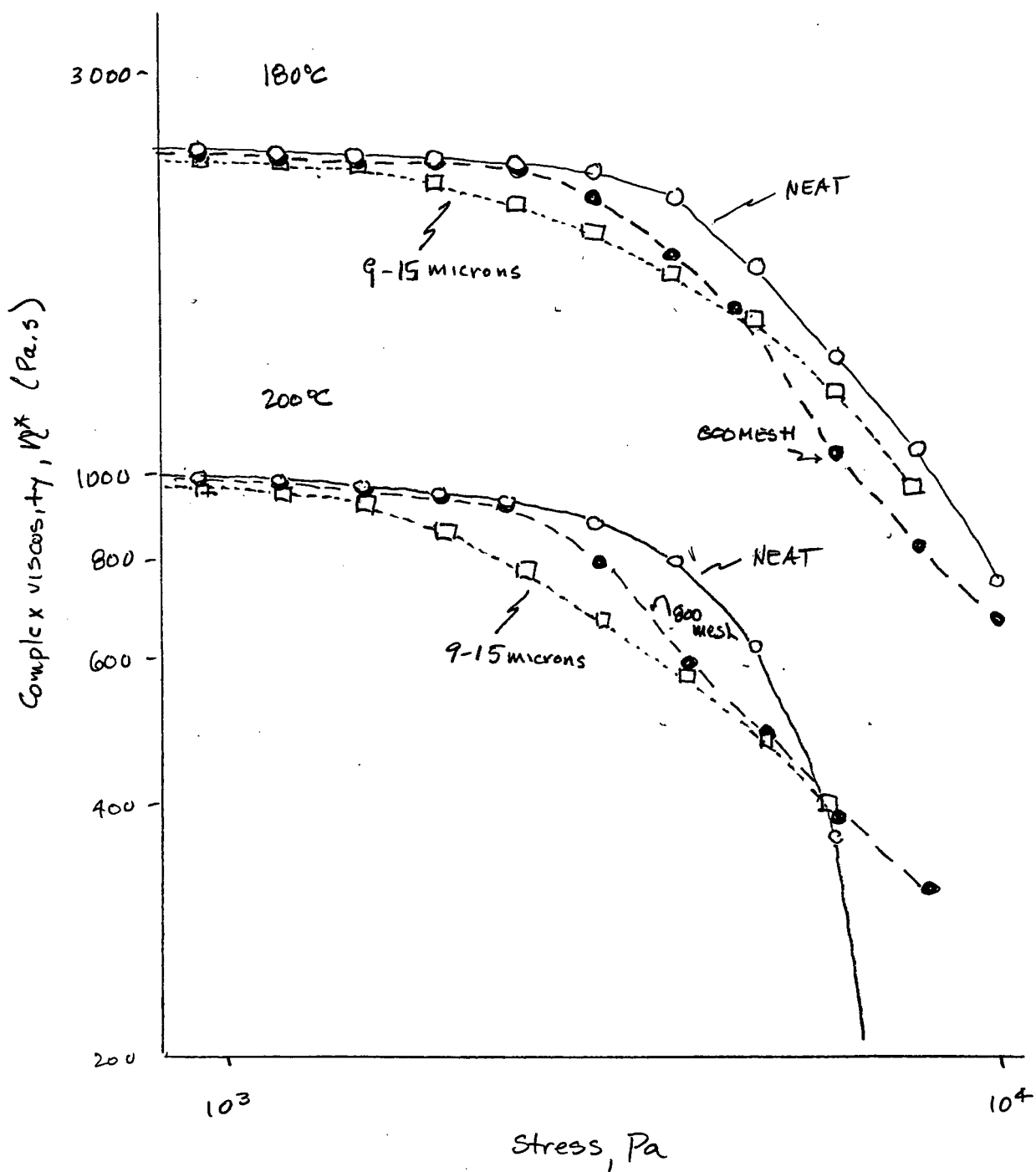


Fig 18. Viscosity of 800-mesh amorphous solid Al as compared to amorphous solid Al classified to 9-15 microns,

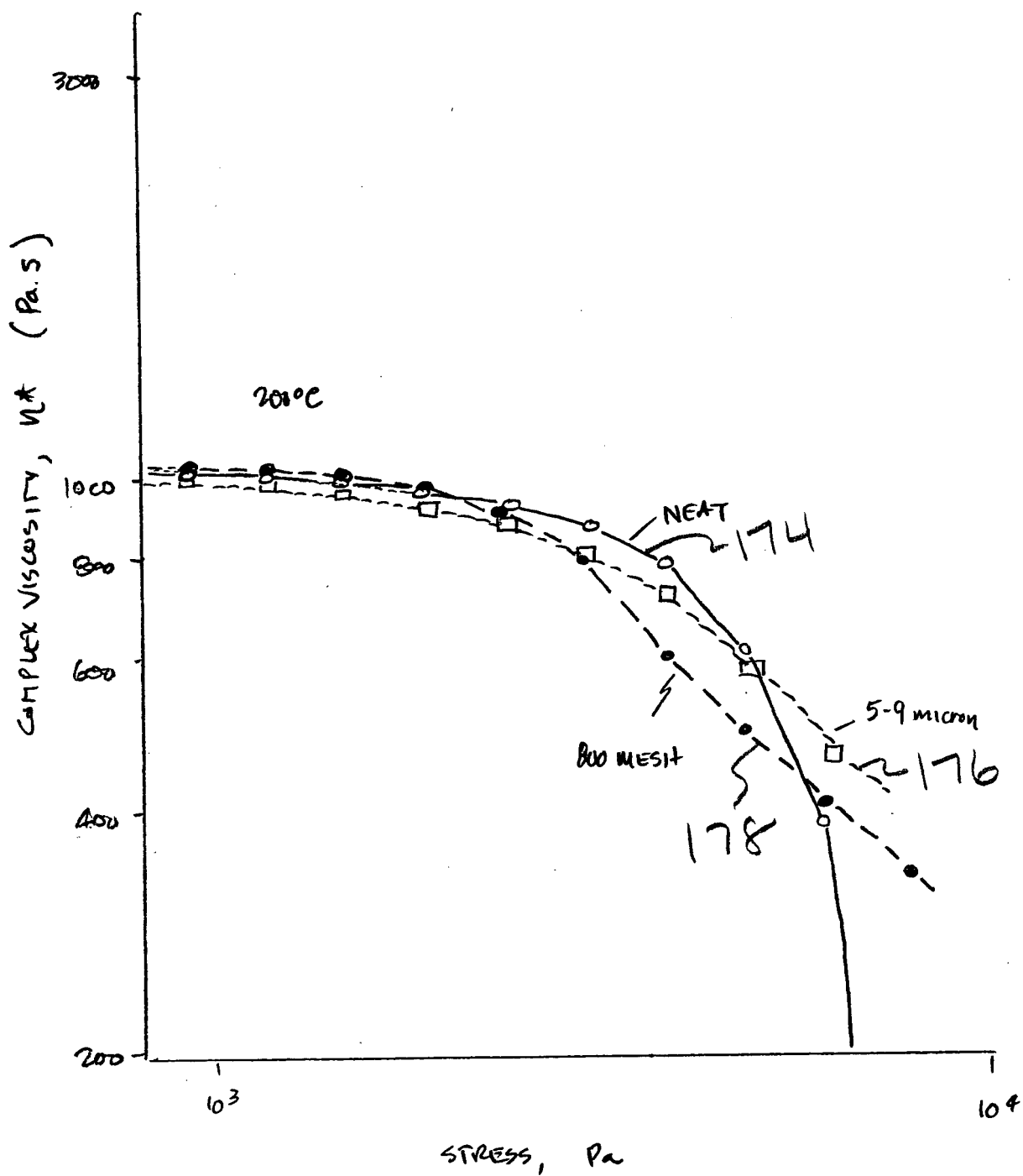


Figure 19. Complex viscosity of 5-9 micron fraction of solid Al.

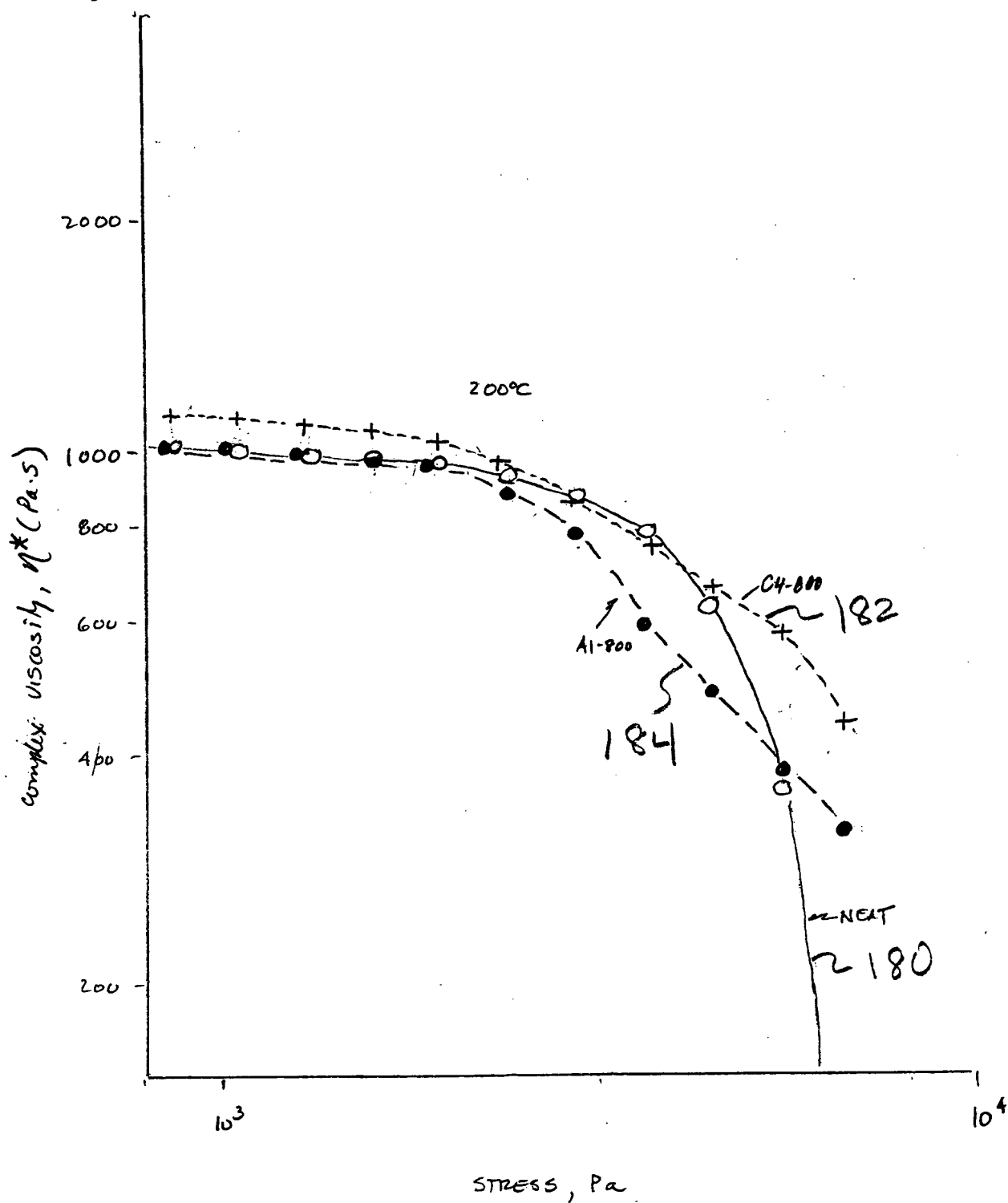


Figure 20. Complex viscosity of amorphous material, A1-800 mesh, crystalline material C4-800 mesh and NEAT PP

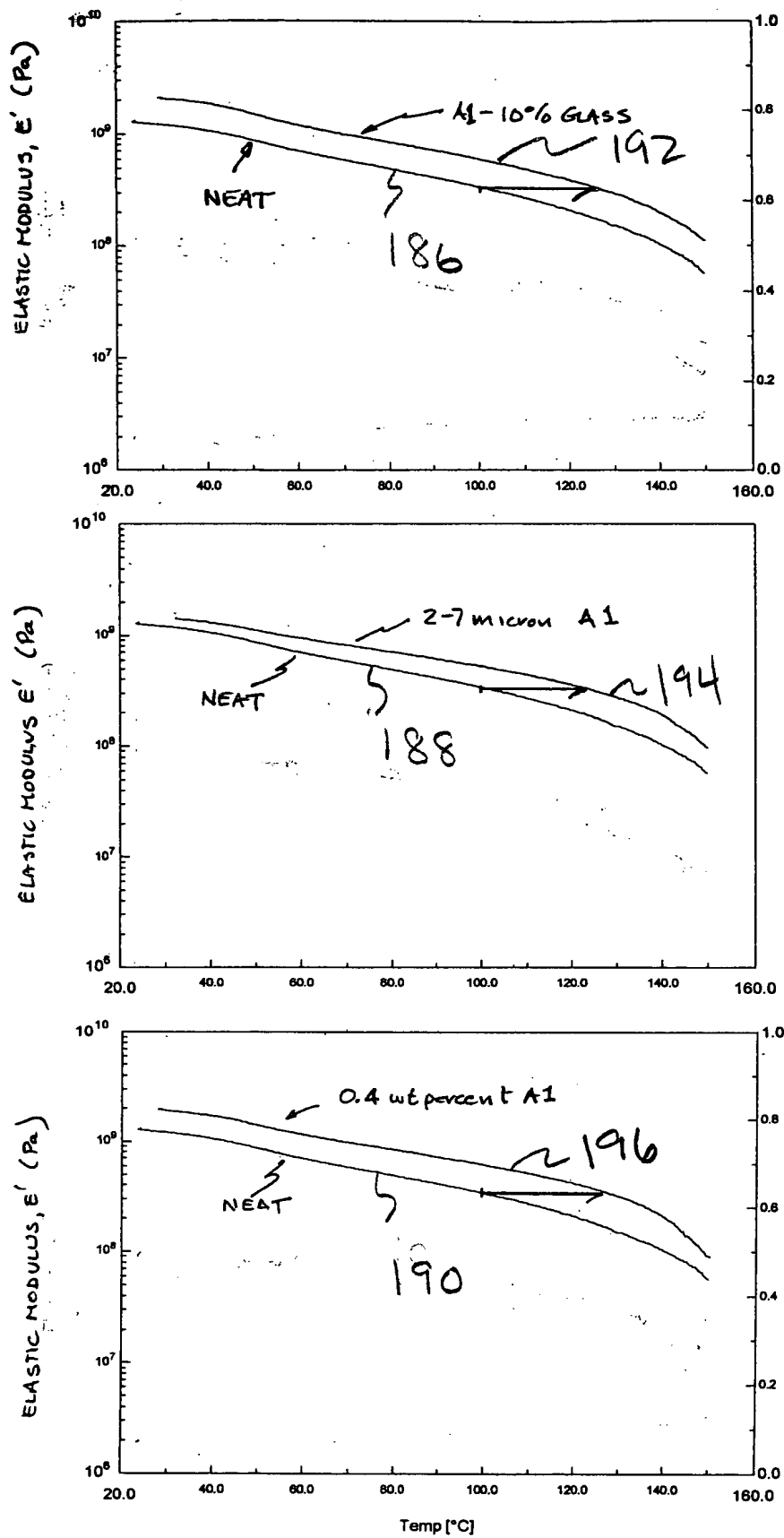


Figure 21. Effect of particle characteristics on dynamic tensile elastic modulus.